Intensities and spectral features of the $^4I_{13/2}$–$^4I_{15/2}$ potential laser transition of Er^{3+} centers in CaF_2–CeF_3 disordered crystal*

Qing-Guo Wang(王庆国)[1,2], Liangbi Su(苏良碧)[3], Jun-Fang Liu(刘军芳)[4], Bin Liu(刘斌)[1], Feng Wu(吴锋)[1,2], Ping Luo(罗平)[1,2], Heng-Yu Zhao(赵衡煜)[1], Jiao-Jiao Shi(施佼佼)[1], Yan-Yan Xue(薛艳艳)[1], Xiao-Dong Xu(徐晓东)[5], Witold Ryba-Romanowski[6], Piotr Solarz[6], Radoslaw Lisiecki[6], Zhan-Shan Wang(王占山)[1], Hui-Li Tang(唐慧丽)[1,2], and Jun Xu(徐军)[1,2,†]

[1] *School of Physics Science and Engineering, Institute for Advanced Study, Tongji University, Shanghai* 200092, *China*

[2] *Shanghai Engineering Research Center for Sapphire Crystals, Shanghai* 201899, *China*

[3] *Key Laboratory of Transparent and Opto-Functional Advanced Inorganic Materials, Shanghai Institute of Ceramics, Chinese Academy of Sciences, Shanghai* 201800, *China*

[4] *School of Materials Science and Engineering, Tongji University, Shanghai* 200092, *China*

[5] *Jiangsu Key Laboratory of Advanced Laser Materials and Devices, School of Physics and Electronic Engineering, Jiangsu Normal University, Xuzhou* 221116, *China*

[6] *Institute of Low Temperature and Structure Research, Polish Academy of Sciences (ILTSR), Okólna*, 50-422 *Wroclaw, Poland*

(Received 4 May 2017; revised manuscript received 21 June 2017; published online 30 September 2017)

A CaF_2–CeF_3 disordered crystal containing 1.06% of Er^{3+} ions was grown by the temperature gradient technique. Optical absorption and emission spectra recorded at room temperature and at 10 K, luminescence decay curve recorded at room temperature, and extended x-ray-absorption fine structure spectra were analyzed with an intention to assess the laser potential related to the $^4I_{13/2} \rightarrow {}^4I_{15/2}$ transition of Er^{3+}. In addition, the thermal diffusivity of the crystal was measured at room temperature. The analysis of room-temperature spectra revealed that the $^4I_{13/2}$ emission is long-lived with a radiative lifetime value of 5.5 ms, peak emission cross section of 0.73×10^{-20} cm^2, and large spectral width pointing at the tunability of the emission wavelength in the region stretching from approximately 1480 nm to 1630 nm. The energies of the crystal field components for the ground and excited multiplets determined from low-temperature absorption and emission spectra made it possible to predict successfully the spectral position and shape of the room-temperature $^4I_{13/2} \rightarrow {}^4I_{15/2}$ emission band. Based on the correlation of the optical spectra and dynamics of the luminescence decay, it was concluded that in contrast to Yb^{3+} ions in heavily doped CaF_2 erbium ions in the CaF_2–CeF_3 crystal reside in numerous sites with dissimilar relaxation rates.

Keywords: laser materials, crystal growth, excited states

PACS: 42.70.Hj, 81.10.Fq, 78.47.da **DOI:** 10.1088/1674-1056/26/11/114208

1. Introduction

Calcium fluoride (CaF_2) has been used as a host crystal for rare earth ions in numerous pioneer works on solid-state lasers that appeared in the early sixties of the past century. Following demonstration of the laser action in CaF_2 doped with Sm^{2+},[1] considerable attention has been paid to spectroscopic and laser properties of trivalent rare earth ions, mainly Nd^{3+} ions in CaF_2[2] and in a variety of mixed compounds CaF_2–YF_3[3] and CaF_2–REF_3 (RE = Ce, La, Gd).[4,5] These early works revealed that the manufacture of calcium fluoride crystals having excellent optical quality and large volume is relatively easy and not expensive. However, the problem of charge compensation occurs when they are doped with trivalent rare earth ions.

It was observed that at a very low concentration rare earth ions reside in isolated centers with cubic, tetragonal, and trigonal site symmetries differing in number and spatial arrangement of ligands. With increasing the concentration, more complex chromophoric centers consisting of dimers are created, and eventually large clusters appear when the rare earth concentration is in the range of tens of percent. In addition, it was found that the distribution of rare earth ions in different chromophoric centers depends on the radii of rare earth ions and on their concentration. In mixed compounds mentioned above, the inherent structural disorder brings about a significant inhomogeneous broadening of spectral lines, and the nature of rare earth sites is even more difficult to determine. In one of the early works, it was concluded that incorporation of YF_3 to CaF_2 results in the creation of new types of centers.[6] However, in a subsequent work, it was concluded that the presence

*Project supported by Shanghai Engineering Research Center for Sapphire Crystals, China (Grant No. 14DZ2252500), the Fund of Key Laboratory of Optoelectronic Materials Chemistry and Physics Chinese Academy of Sciences (Grant No. 2008DP17301), the Fundamental Research Funds for the Central Universities of China, the National Natural Science Foundation of China and China Academy of Engineering Physics Joint Fund (Grant No. U1530152), the National Natural Science Foundation of China (Grant Nos. 61475177 and 61621001), the Natural Science Foundation of Shanghai Municiple, China (Grant No. 13ZR1446100), and the MOE Key Laboratory of Advanced Micro-Structured Materials of China.

†Corresponding author. E-mail: xujun@mail.shcnc.ac.cn

© 2017 Chinese Physical Society and IOP Publishing Ltd

of YF_3 affects merely the distribution of rare earth ions over existing centers in CaF_2.[7] In view of these problems, CaF_2 crystals doped with trivalent rare earth ions have not been regarded as promising laser materials during several decades. In fact, fundamental spectroscopic parameters relevant to the laser performance of a CaF_2:Nd system have been reported quite recently.[8]

Renewal of the interest in these systems that occurred over the course of several years is related to the search for broad-band emitting materials for the design of all-solid-state high-power ultrafast lasers. In a recent paper, advantages and drawbacks of CaF_2:Yb^{3+} systems, denoted by authors as "a new old laser crystal," have been revised and compared to other ytterbium-doped crystals that may be of interest for this purpose.[9] Taking into account the performance of CaF_2:Yb^{3+} high-power and/or femtosecond lasers reported in numerous papers published during the last ten years, the authors have underlined the importance of this material for practical application.

In contrast to the knowledge of CaF_2:Yb^{3+} on the laser potential of erbium-doped CaF_2 crystals is rather poor. In several early papers, spectroscopic features[10] were reported, and the feasibility of laser action associated with the $^4S_{3/2} \rightarrow {}^4I_{13/2}$ transition at approximately 850 nm and with the $^4I_{11/2} \rightarrow {}^4I_{13/2}$ transition at approximately 2.69 μm at cryogenic temperatures was demonstrated.[11] Recently, a laser operation associated with the $^4I_{11/2} \rightarrow {}^4I_{13/2}$ transition of Er^{3+} in CaF_2 at approximately 2.8 μm has been observed at room temperature upon optical pumping at 800 nm and 975 nm with a Ti-sapphire laser and at 1520 nm with a color center laser.[12] However, laser operation on the $^4I_{13/2} \rightarrow {}^4I_{15/2}$ transition at approximately 1.6 μm was a significant problem since a large energy gap between the $^4I_{11/2}$ level and the $^4I_{13/2}$ level, combined with a relatively low energy of lattice vibration of the CaF_2 host, results in a small multiphonon relaxation rate thereby preventing the energy flow to the $^4I_{13/2}$ level from higher energy pump levels. As a consequence, a practically significant population inversion cannot be obtained, unless the $^4I_{13/2}$ level is resonantly pumped. These findings were not encouraging. Nevertheless, a recent discovery of an efficient energy transfer process between Er^{3+} and Ce^{3+} that is able to drastically enhance the energy flow from the $^4I_{11/2}$ level to the $^4I_{13/2}$ level of erbium[13] may open new means to overcome the problem. In fact, recent investigation of Yb/Er:CeF_3 nanoparticles synthesized by the hydrothermal process revealed a high efficiency of 1.5 μm emission upon exciting at 975 nm without visible up-conversion luminescence.[14] Additionally, it was demonstrated that the rate of the $^4I_{11/2} \rightarrow {}^4I_{13/2}$ transition in an Er/Yb/Na/Ce:CaF_2 crystal was enhanced by about 40 times by the deactivating effect of Ce^{3+}.[15]

Encouraged by the findings above, we investigate the fundamental properties of an erbium-doped CaF_2–CeF_3 (Ca:Ce = 2:1) disordered crystal, which are relevant to the laser performance at approximately 1.6 μm. In our previous paper,[16] preliminary spectroscopic data on erbium-doped as well as erbium and ytterbium co-doped CaF_2–CeF_3 consisting of the Judd–Ofelt treatment, room-temperature luminescence spectra calibrated in terms of arbitrary units, and decay curves were reported. In the present work, we report a more detailed and comprehensive investigation of a CaF_2–CeF_3 crystal single-doped with Er^{3+} ions. First, the Judd–Ofelt analysis was refined considering the contribution of the magnetic dipole (MD) mechanism to both absorption and emission transitions. Next, the emission cross section and gain coefficient as functions of the wavelength for the $^4I_{13/2} \rightarrow {}^4I_{15/2}$ transition were evaluated. In subsequent sections, we present and discuss low-temperature optical spectra and results of extended x-ray-absorption fine structure (EXAFS) and thermal conductivity measurements. As far as we know, the information gathered in this work has not been reported before. The results obtained in this study are discussed with reference to the data for a CaF_2:Er^{3+} system reported in Refs. [7] and [17].

2. Experimental

Crystal CaF_2–CeF_3 doped with Er^{3+} was grown by the temperature gradient technique (TGT) described in Ref. [18]. The raw materials (CaF_2, CeF_3, ErF_3, and PbF_2) were mixed according to the chemical ratios and put into the sealed graphite crucible. The ratio of CeF_3 and CaF_2 was 1:2. The PbF_2 (1 mol%) powder was used as the oxygen scavenger. The mixtures were melted at 1400 °C and then grown on ⟨111⟩ CaF_2 seeds with reducing the temperature at a cooling rate of ∼ 5 °C/h. In this way, the CaF_2–CeF_3 transparent crystal with Er^{3+} was obtained. The erbium concentrations at different parts of the grown crystal were checked by the inductively coupled plasma atomic emission spectrometry analysis. It was found that the actual concentration of Er^{3+} in the grown crystal was significantly lower than the original one (1.4%) implying that the segregation coefficient is inferior to unity. To obtain meaningful spectroscopic data, the Er^{3+}concentration in the part of the crystal adjacent to a sample was measured to be 1.06%, which is equivalent to 1.66×10^{20} Er^{3+} ions per cubic centimeter.

The absorption spectra of the crystal were recorded with a Varian Model 5E UV-visible-near-IR (UV-VIS-NIR) absorption spectrophotometer at 10 K and 300 K. The spectral bandwidth of the spectrophotometer was set to 0.1 nm in the UV-VIS region and to 0.2 nm in the NIR region. The emission spectra at 300 K and at 10 K were excited by an argon ion laser at 514 nm and recorded with the Dongwoo Optron monochromator DM 711 with a focal length of 750 mm, coupled to a

cooled InGaAs infrared detector. For low-temperature measurements, the sample was put into an Oxford Model CF 1204 continuous flow liquid helium cryostat equipped with a temperature controller.

EXAFS data were obtained using a facility available in the National Synchrotron Radiation Laboratory, University of Science and Technology of China. Measurements were made at room temperature at the Er L-edge (8794 eV) and in the fluorescence mode, owing to the low contentment of erbium in the crystal, by using a Si (111) double crystal monochromator. The XAFS measurements were conducted in the nonfocused mode, and the corresponding spot diameter was $> 1 \times 1$ mm^2. The XAFS spectra were recorded from 8794 eV to 9933 eV, every 0.5 eV with a 5 s accumulation time per point. All the spectra were normalized in the same way using Athema[19] software.

The thermal diffusivity of the material was measured with an LFA-427 laser flash diffusivity apparatus (NETZSC Ltd, Germany). The laser pulse intensity was 0–20 J, pulse width between 0.2 ms and 1.2 ms. For this measurement, a sample in the form of a disk 10 mm in diameter and 1.7 mm thick was prepared.

3. Results and discussion

3.1. Room-temperature optical spectra and transition intensities

A survey absorption spectrum recorded at room temperature for the CaF_2–CeF_3 crystal containing 1.06% of Er^{3+} is shown in Fig. 1. Broad unresolved spectral bands that appear in the spectrum show an inhomogeneous broadening characteristic for rare earth ions embedded in the crystal lattices with significant structural disorder.

From the room-temperature absorption spectrum, the peak absorption cross section of the $Er^{3+4}I_{15/2} \rightarrow {}^4I_{13/2}$ transition is calculated to be approximately 0.72×10^{-20} cm^{-2} with the equation

$$\sigma_{\text{abs}} = \frac{2.303 \lg I_0/I}{LN},$$

where L is the thickness of the sample, N is the concentration of the Er^{3+} ions (cm^{-3}), and $\lg I_0/I$ is the absorption light density.

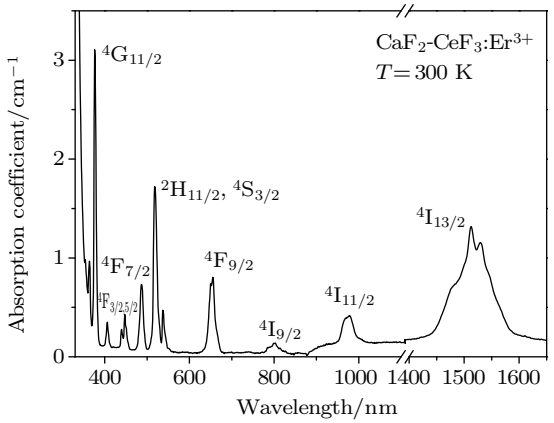


Fig. 1. Survey absorption spectrum of Er-doped CaF_2–CeF_3 recorded at 300 K.

The transition intensities for the Er^{3+}:CaF_2–CeF_3 system were analyzed within a framework of the standard Judd–Ofelt approach.[20,21] The experimental oscillator strengths f_{exp} for the absorption transitions were determined by a numerical integration of the absorption bands shown in Fig. 1. The Judd–Ofelt theory accounts for electric dipole (ED) transitions. Magnetic dipole MD transitions obey selection rules $\Delta L = 0$, $\Delta S = 0$, $\Delta J = 0, 1$ (except for $0 \leftrightarrow 0$). Therefore, the contribution of the MD mechanism to the ${}^4I_{15/2} \rightarrow {}^4I_{13/2}$ absorption intensity was evaluated and next subtracted from the experimental oscillator strength f_{exp} for this transition prior to the fitting procedure. To determine intensity parameters Ω_t, a set of ten experimental f_{exp} values were used as input data in the procedure of fitting the experimental and theoretical oscillator strengths by the least squares technique. The expression for theoretical oscillator strengths was constructed using the reduced matrix elements from Ref. [22]. The results of the fitting are gathered in Table 1.

Table 1. Experimental and theoretical oscillator strengths of Er^{3+} transitions in the CaF_2–CeF_3:Er^{3+} crystal.

${}^4I_{15/2} \rightarrow S'L'J'$	λ_{abs}/nm	FWHM/nm	$\int \text{OD}(\lambda)\,\text{d}\lambda$	$f_{\text{exp}}/10^{-6}$	$f_{\text{md}}/10^{-6}$	$f_{\text{ed}}/10^{-6}$	$f_{\text{cal}}^{\text{ed}}/10^{-6}$	$\Delta/10^{-6}$
${}^4I_{13/2}$	1513	70	11.29279	2.8727	0.4407	2.4320	2.3038	0.1282
${}^4I_{11/2}$	978	33	2.68259	1.6332	–	1.6332	1.0283	0.6049
${}^4I_{9/2}$	803	34	0.68873	0.6220	–	0.6220	0.1525	0.4695
${}^4F_{9/2}$	655	15	1.62774	2.2094	–	2.2094	2.1257	0.0837
${}^4S_{3/2}$, ${}^2H_{11/2}$	518	9	2.52677	5.4837	–	5.4837	5.5916	0.1079
${}^4F_{7/2}$	487	9	0.79034	1.9406	–	1.9406	3.1978	1.2572
${}^4F_{5/2,3/2}$	447	7	0.45222	1.3180	–	1.3180	1.8431	0.5251
${}^2H_{9/2}$	406	6	0.21066	0.7442	–	0.7442	1.3331	0.5889
${}^4G_{11/2}$	376	5	1.98632	8.1817	–	8.1817	8.1256	0.0561
${}^4G_{9/2}$	364	4	0.23893	1.0501	–	1.0501	1.1777	0.1276
$\Omega_2 = 3.1340 \times 10^{-20}$ cm^2; $\Omega_4 = 0.6649 \times 10^{-20}$ cm^2; $\Omega_6 = 2.7302 \times 10^{-20}$ cm^2 RMS $= 0.5621 \times 10^{-6}$								

The Judd–Ofelt parameters determined during the fitting procedure were next used to evaluate the rates of ED transitions originating in the $^4I_{13/2}$ and $^4I_{11/2}$ excited states. Next, the calculated MD transition rates were added to obtain the total transition rates, corresponding radiative lifetimes, and luminescence branching ratios relevant to the laser operation of Er^{3+} in the CaF_2–CeF_3 matrix. The results of the calculation are given in Table 2.

Table 2. Radiative transition probabilities A, radiative lifetimes τ_{rad}, and branching ratios of luminescence β determined for selective Er^{3+} transitions in the CaF_2–CeF_3:Er crystal.

Tansitions	E/cm^{-1}	A_{ed}/s^{-1}	A_{md}/s^{-1}	A/s^{-1}	β/%
$^4I_{13/2} \rightarrow {}^4I_{15/2}$	6500	151.7	29.6	181.3	100
$^4I_{11/2} \rightarrow {}^4I_{13/2}$	3600	217	7.8	295.	13.7
$^4I_{15/2}$	10100	188.5	–	188.5	86.3
τ_{rad} ($^4I_{13/2}$) = 5.5 ms, τ_{rad} ($^4I_{11/2}$) = 4.6 ms					

The Judd–Ofelt parameters Ω_t mentioned above differ slightly from those reported in Ref. [16] since in contrast to the previous calculation, the contribution of MD transition was included. The same applies to the calculated values of the radiative transition rates and radiative lifetimes gathered in Table 2.

The comparison of the values in Tables 1 and 2 with those reported in Ref. [17] for a CaF_2 crystal containing 0.1% of Er^{3+} reveals that the intensities of the absorption transitions in the two systems are within the same order of magnitude. However, the dissimilarity between the Judd–Ofelt parameters $\Omega_2 = 6.6 \times 10^{-20}$ cm^2, $\Omega_4 = 2.3 \times 10^{-20}$ cm^2, and $\Omega_6 = 2.0 \times 10^{-20}$ cm^2 reported for CaF_2:Er^{3+} systems and those for Er^{3+} in the CaF_2–CeF_3 matrix is significant.

The energy between the $^4I_{11/2}$ and $^4I_{13/2}$ multiplets of Er^{3+} ions is approximately 3600 cm^{-1}, which is almost the same as the band gap between the $^2F_{5/2}$ and $^2F_{7/2}$ energy level of Ce^{3+} ions.[16] Therefore, the decay of the $^4I_{11/2} \rightarrow {}^4I_{13/2}$ transition of Er^{3+} ions would be significantly improved through the resonant energy transfer from Er^{3+} ions and Ce^{3+} ions. The improvement of the decay rate corresponding to the $^4I_{13/2}$ multiplet of Er^{3+} ions can reduce the excited state absorption and even the clusters of Er–Er ions. Figure 2 shows the details of the $^4I_{15/2} \rightarrow {}^4I_{13/2}$ absorption band and of the $^4I_{13/2} \rightarrow {}^4I_{15/2}$ emission band recorded at room temperature. The shown emission band was calibrated in terms of the emission cross section units using the Fuchtbauer–Ladenburg relation

$$\sigma_{em}(\lambda) = \frac{\beta\lambda^5}{8\pi c n^2 \tau_{R2}} \times \frac{I(\lambda)}{\int I(\lambda)\lambda \, d\lambda},$$

where β is the branching ratio (for the $^4I_{13/2}$ level, $\beta = 1$); n is the refraction index of the crystal, which is measured to be approximately 1.50; τ_{R2} is the radiative lifetime of the $^4I_{13/2}$ level, which is calculated to be 5.5 ms using the J–O theory; and $I(\lambda)$ represents the experimental emission intensity as a function of the wavelength λ.

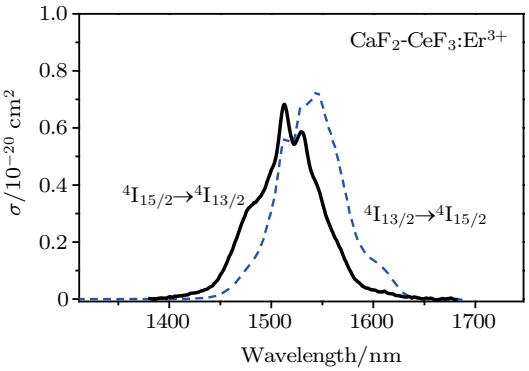


Fig. 2. Absorption cross section and emission cross section correspond to the $^4I_{15/2} \rightarrow {}^4I_{13/2}$ and $^4I_{13/2} \rightarrow {}^4I_{15/2}$ transitions of Er^{3+} in CaF_2–CeF_3:Er^{3+}.

It may be interesting to compare peculiarities of the $^4I_{13/2} \rightarrow {}^4I_{15/2}$ emission presented above with those reported for a CaF_2 crystal containing 0.01% of Er^{3+}.[17] Owing to a small doping level, erbium ions in this sample are likely to enter isolated centers.[23,24] The reported $^4I_{13/2} \rightarrow {}^4I_{15/2}$ emission spectrum contains four local maxima at 1460, 1505, 1522, and 1540 nm; nevertheless, the overall width of this spectrum is nearly the same as that recorded for our CaF_2–CeF_3:Er^{3+} sample. In addition, the spectral positions of the band maximum for the two systems differ by several nanometers only. From this comparison, it follows that the diversity of transition energy values for different Er^{3+} centers that contribute to the broad-band emission in the CaF_2–CeF_3:Er^{3+} system is small.

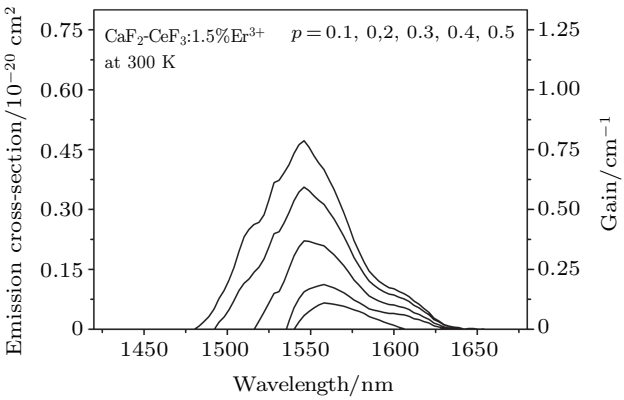


Fig. 3. Effective emission cross section and gain as a function of the wavelength for different values of the population inversion parameter p.

It can be seen from Fig. 2 that the peak emission cross section at $\sim$ 1544 nm is 0.73×10^{-20} cm^2. When considering the laser potential in this spectral region, the adverse effect of the self-absorption should be accounted for. For this purpose, we follow the commonly used approach and calculate the effective emission cross section as a function of the wavelength $\sigma_{eff}(\lambda)$ using the relation $\sigma_{eff} = p\sigma_{em}(\lambda) - (1-p)\sigma_{abs}(\lambda)$,

where p is the population inversion parameter, defined as the density of excited Er^{3+} ions divided by the overall erbium concentration N_0. Figure 3 shows the plots of $\sigma_{\text{eff}}(\lambda)$ as a function of the wavelength calculated for p values ranging from 0.1 to 0.5. From these plots, it follows that the gain $g(\lambda)$ defined as $g(\lambda) = N_0\sigma_{\text{eff}}(\lambda)$ will be positive even for the p parameter as low as 0.1. For $p = 0.5$, a reasonable value likely to be encountered in practice, a broad spectral range of the potential laser operation stretching from about 1480 nm to 1630 nm is predicted for the Er-doped CeF_3–CaF_2 disordered crystal.

3.2. Nature of Er^{3+} sites in the CaF_2–CeF_3 matrix

The above-described analysis of the transition intensities and the calibration of the absorption and emission bands were performed for broad unresolved optical spectra that contain, in principle, contributions from all different Er^{3+} centers, whatever their number and types are. However, when considering the laser potential of such a disordered material, the question whether among numerous Er^{3+} centers a dominant one exists is of crucial importance. An outstanding laser potential of a CaF_2 crystal heavily doped with Yb^{3+} stems from the fact that almost all ytterbium ions reside in only one kind of center (hexameric type) rather than in various isolated and dimer centers that are encountered when the Yb^{3+} concentration is small.[25–28] To get a closer insight into the nature of Er^{3+} sites in the CaF_2–CeF_3 matrix, optical spectra were recorded at a low temperature and examined carefully. Figure 4 shows the details of the absorption bands related to the transitions from the ground $^4I_{15/2}$ multiplet to the excited $^4S_{3/2}$, $^4F_{5/2}$, and $^4F_{3/2}$ multiplets recorded at 10 K.

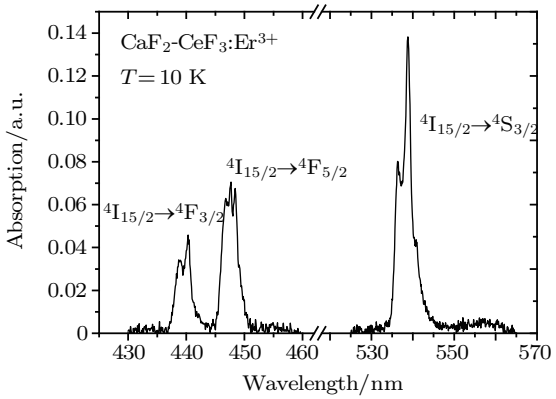


Fig. 4. Absorption bands assigned to the $^4I_{15/2} \rightarrow ^4S_{3/2}$, $^4F_{5/2}$, and $^4F_{3/2}$ transitions of Er^{3+}recorded at $T = 10$ K.

At $T = 10$ K, the kT value is ~ 7 cm^{-1}. Thus, one can expect that the lowest crystal field component of the ground $^4I_{15/2}$ multiplet solely will have a population high enough to contribute to the absorption transitions. For each particular Er^{3+} center, two crystal field components of the $^4S_{3/2}$ and $^4F_{3/2}$ multiplets and three crystal field components of the $^4F_{5/2}$ multiplet are predicted (neglecting isolated centers with O_h symmetry). It can be seen in Fig. 4 that the band related to the $^4I_{15/2} \rightarrow ^4F_{3/2}$ transition contains two components peaking at 437 nm and 440 nm, and the band related to the $^4I_{15/2} \rightarrow ^4F_{5/2}$ transition contains three components peaking at 447, 448, and 449 nm. In the band related to the $^4I_{15/2} \rightarrow ^4S_{3/2}$ transition, two intense components peaking at 536 nm and 539 nm are clearly seen, and a weaker third component at 541 nm can be discerned. Although the number of band components in these spectra complies with the number of crystal field components of the terminal multiplets, the overall spectral widths of the bands is large (between 5 nm and 10 nm) indicating that we observe the superposition of numerous transitions having slightly different energy. There is a striking similarity between the low-temperature spectra shown above and the corresponding absorption spectra at 77 K for the CaF_2 crystal containing 1% of Er^{3+} and for the CaF_2 crystal containing Er^{3+} and YF_3 with a concentration up to 2% reported in Ref. [7]. This early study revealed that for an Er^{3+} concentration of 0.01%, absorption spectra related to the $^4I_{15/2} \rightarrow ^4F_{5/2}$ and $^4I_{15/2} \rightarrow ^4S_{3/2}$ transitions consist of several very narrow lines, but when the Er^{3+} concentration increased to 1%, the intensity of narrow lines disappeared almost completely in favor of new broad bands, each of them having the overall spectral width of about 2 nm and two local maxima. Similar spectra were observed for the CaF_2 crystal containing a much smaller content of Er^{3+}, but containing an admixture of YF_3, and this finding led to the conclusion that the spectra are affected by the sum of the ErF_3 and YF_3 concentrations rather than the Er^{3+} concentration alone. In our crystal, the sum of the CeF_3 and ErF_3 concentrations is considerably higher than that in the system mentioned above. Resulting structural disorder induces strong inhomogeneous broadening of absorption bands, but weakly affects the spectral positions of the band maxima. Figure 5 shows the absorption spectrum related to the $^4I_{15/2} \rightarrow ^4I_{13/2}$ transition of Er^{3+}in the CaF_2–CeF_3 crystal recorded at 8 K. After the Gaussian fitting process, it was found that the band consists of seven components (as shown in Fig. 5). The crystal field splitting of the $Er^{3+4}I_{13/2}$ manifold was determined from this spectrum.

Valuable information regarding the nature of rare earth sites in crystal hosts can be obtained usually from low-temperature luminescence spectra. Unfortunately, attempts to record spectra of luminescence originating in the $^4S_{3/2}$, $^4F_{9/2}$, $^4I_{9/2}$, and $^4I_{11/2}$ levels of Er^{3+} in our crystal both at room temperature and at 10 K were unsuccessful because emission from the levels higher than $^4I_{13/2}$ is completely quenched by Ce^{3+} ions. Figure 6 shows the low-temperature spectrum related to the $^4I_{13/2} \rightarrow ^4I_{15/2}$ transition of Er^{3+} in the CaF_2–CeF_3 matrix. An argon ion laser emitting at 514 nm was used as an excitation source, and the spectral resolution of

an emission monochromator used was set to 0.1 nm. Assignment of the band components indicated in the figure was made by Gaussian fitting with reference to the crystal field splitting of the $^4I_{13/2}$ multiplet mentioned above. Some comments are needed to account for an assignment of the band component on the high-energy side of the spectrum to transitions originating from the second and third crystal field levels of the $^4I_{13/2}$ multiplet. If the temperature of the excited region of the crystal sample amounted actually to 10 K, these transitions should be negligibly weak. However, in contrast to the absorption spectra measurement, the power dissipated in a small region of the sample excited with a focused laser beam may result in a local increase in the sample temperature, especially when the thermal conductivity of the crystal is small (vide infra).

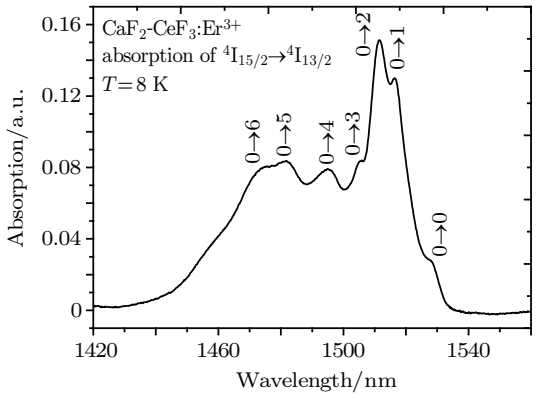


Fig. 5. Absorption band related to the $^4I_{15/2} \rightarrow {}^4I_{13/2}$ transition of Er^{3+} ions in the CaF_2–CeF_3 crystal at 8 K.

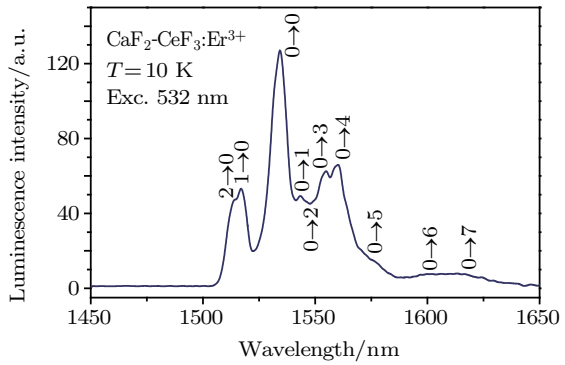


Fig. 6. Low-temperature luminescence spectrum of the Er^{3+} $^4I_{13/2} \rightarrow {}^4I_{15/2}$ transition in the CaF_2–CeF_3 crystal excited at 514 nm.

Table 3 summarizes the energies of the crystal field levels for the $^4I_{13/2}$ and $^4I_{15/2}$ multiplets of Er^{3+} ions in the CaF_2–CeF_3 crystal as determined from the low-temperature absorption and emission spectra. To check the reliability of the data in Table 3 above, we evaluated the room-temperature $^4I_{13/2} \rightarrow {}^4I_{15/2}$ emission band by the so-called reciprocity method that relays on the measured $^4I_{15/2} \rightarrow {}^4I_{13/2}$ absorption spectrum according to the relation

$$\sigma_{\mathrm{em}}(\lambda) = \frac{Z_{\mathrm{low}}}{Z_{\mathrm{up}}}\sigma_a(\lambda)\exp\left(\frac{Z_{\mathrm{ZL}} - E(\lambda)}{k_{\mathrm{B}}T}\right),$$

where $\sigma_{\mathrm{a}}(\lambda)$ is the absorption cross section and Z_{low} and Z_{up} are the partition functions for the lower and upper states, respectively, defined as

$$Z_{\mathrm{low}} = \sum_{i=1}^{n} g_i \exp\left(\frac{-E_i}{k_{\mathrm{B}}T}\right),$$
$$Z_{\mathrm{up}} = \sum_{j=1}^{n} g_j \exp\left(\frac{-(E_j - E(\lambda))}{k_{\mathrm{B}}T}\right),$$

where $g_i(g_j)$ are the degeneracies of the crystal field levels, $E_i(E_j)$ are the energies of the crystal field levels, E_{ZL} is the energy separation between the lowest crystal field levels of the upper and lower states, and k_{B} is the Boltzmann constant.

Table 3. Energies of the crystal field levels (in cm^{-1}) of Er^{3+} ions in the CaF_2–CeF_3 disordered crystal.

Er^{3+} manifold	Sublevel N^0								ΔE
	0	1	2	3	4	5	6	7	
$^4I_{15/2}$	0	47	73	106	135	192	295	353	353
$^4I_{13/2}$	6545	6596	6618	6645	6693	6752	6780	–	235

Figure 7 compares the spectra obtained by the reciprocity method defined above and by the Fuchtbauer–Ladenburg method described in the previous section. It can be seen in this figure that the agreement between the spectra is surprisingly good. The results presented above seem to indicate that in spite of the structural disorder, a majority of erbium ions reside in one kind of site, an analogue of hexomeric sites reported for a CaF_2 crystal heavily doped with Yb^{3+} ions. However, the recorded decay curve of the $^4I_{13/2}$ emission does not corroborate this supposition.

Figure 8 shows the semilog plot of the $^4I_{13/2}$ luminescence decay curve recorded at room temperature. It can be seen that in the whole time scale the curve is far from a single exponential time dependence implying that erbium ions having markedly different relaxation rates contribute to the luminescence. As a consequence, the definitive $^4I_{13/2}$ lifetime cannot be determined from this decay curve, and the so-called mean lifetime τ_{mean} defined by the relation

$$\tau_{\mathrm{mean}} = \frac{\int_{t=0}^{\infty} tI(t)\,\mathrm{d}t}{\int_{t=0}^{\infty} I(t)\,\mathrm{d}t},$$

in which I is the intensity of luminescence and t represents time, can be found solely. In this way, $\tau_{\mathrm{mean}} = 3.3$ ms was calculated. The mean lifetime defined above takes into account the contribution of a slower decay in the tail of the decay curve. Thus, its value is slightly higher than the lifetime value of 2.99 ms reported in Ref. [16].

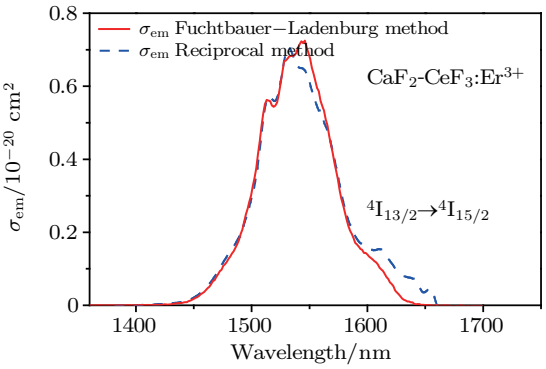


Fig. 7. (color online) Emission cross section $^4I_{13/2} \rightarrow {}^4I_{15/2}$ of Er^{3+} derived by means of the reciprocal and Fuchtbauer–Ladenburg methods.

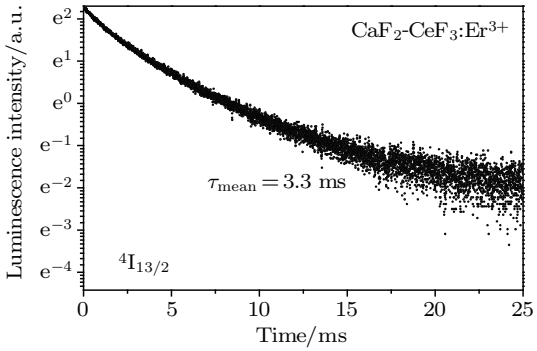


Fig. 8. Decay curve of $^4I_{13/2}$ luminescence of Er^{3+} in CaF_2–CeF_3:Er^{3+}.

An attempt was made to obtain more information from the EXAFS measurement. Figure 9 shows the EXAFS spectra for the Er^{3+}:CaF_2–CeF_3 disordered crystal. Some structural information on the doped ions in the crystal can be obtained by fitting the Fourier transform for the experimental data. It was found that the average coordination number of Er^{3+} ions in the grown crystal is 9.8, which is higher than that in Er^{3+}-CaF_2:8 or 9 at 2.3–2.4 Å,[29] and the average length of [Er–F] bonds is approximately 2.6 Å.

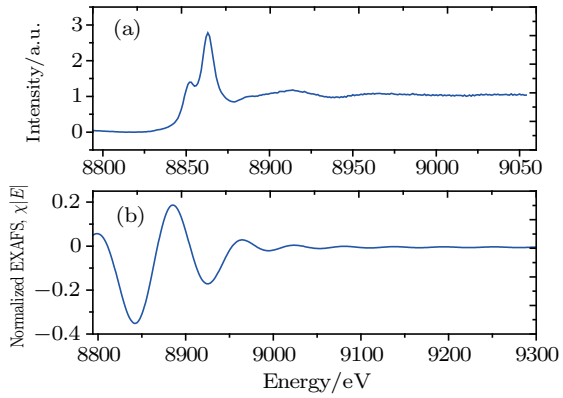


Fig. 9. (color online) EXAFS spectra for the Er-doped CaF_2–CeF_3 disordered crystal. (a) Experimental data and (b) normalized EXAFS.

3.3. Thermal conductivity

The thermal diffusion coefficient η of our sample was measured to be 0.00444 cm^2/s. From this value, the thermal conductivity k was calculated using the equation $k = \eta\rho C_p$, where k, η, ρ, and C_p denote the thermal conductivity, thermal diffusion coefficient, density, and the specific heat of the crystal, respectively. By inserting the values of $\rho = 4.8$ g/cm^3 and $C_p = 854$ J/(kg·K) to the equation above, the thermal conductivity of the crystal was calculated to be 1.82 W/(m·K). The obtained value of the thermal conductivity is small. The thermal conductivity of the undoped CaF_2 single crystal was measured to be 9.71 W/(m·K).[30] Upon doping with rare earth ions, the thermal conductivity decreases because incorporated ions act as point defects affecting adversely the mean free path of phonons. For the CaF_2 crystal heavily doped with Yb^{3+} (2.59 %), it amounts to 5.4 W/(mK).[9] In spite of a smaller Er^{3+} concentration, the degree of disorder in the CaF_2–CeF_3 crystal is markedly higher, and therefore its thermal conductivity is poor. The thermal properties can be improved by the optimization of the doping concentration, and in general, the Er^{3+}:CaF_2–CeF_3 disordered crystal is a promising candidate for broad-band laser operation from 1480 nm to 1630 nm.

4. Conclusions

The properties of the CaF_2–CeF_3 (Ce : Ca = 1 : 2) disordered crystal containing 1.06% of Er^{3+} grown by the TGT, relevant to potential laser operation near 1.6 μm, were investigated. The analysis of the room-temperature optical absorption and emission spectra made it possible to reveal that the system under study shows advantageous spectroscopic features such as broad absorption bands suitable for optical pumping, a broad emission band related to the potential $^4I_{13/2} \rightarrow {}^4I_{15/2}$ laser transition, and a long radiative lifetime $\tau_{rad} = 5.5$ ms of the $^4I_{13/2}$ upper laser level. The evaluated peak value for the $^4I_{13/2} \rightarrow {}^4I_{15/2}$ emission cross section of 0.73×10^{-20} cm^2 indicates that the system under study can be considered as an intermediate-gain laser material, and the gain coefficient calculated considering the phenomenon of self-absorption predicts a large spectral region of laser emission stretching from approximately 1480 nm to 1630 nm. The analysis of the low-temperature spectra of the Er-doped CaF_2–CeF_3 crystal with reference to the low-temperature spectra reported for a CaF_2 crystal heavily doped with Er^{3+} and co-doped with Er^{3+} and Y^{3+} revealed that the large content of CeF_3 in the system under study brings about a significant broadening of spectral bands, but weakly influences their spectral positions and the distribution of band components implying similar nature of Er^{3+} centers in the two systems. The energies of the crystal field levels determined from the low-temperature absorption and emission spectra made it possible to predict successfully the spectral position and shape of the $^4I_{13/2} \rightarrow {}^4I_{15/2}$ emission band at 300 K leading to the supposition that a majority of Er^{3+} ions reside in one kind of centers, an analogue of Yb^{3+} centers in a heavily doped

CaF_2 crystal. However, this supposition has been corroborated by the measurement of the luminescence decay curve, which showed a strong deviation from a single exponential time dependence. From the EXAFS spectra, it was derived that the average coordination number of Er^{3+} ions in the grown crystal is 9.8 and the average length of [Er–F] bonds is approximately 2.6 Å. Thus, the occurrence of numerous dissimilar Er^{3+} centers and low thermal conductivity are serious shortcomings that may influence adversely the laser potential of an erbium-doped CaF_2–CeF_3 crystal.

References

[1] Kaiser W, Garret C and Wood D 1961 *Phys. Rev.* **123** 766
[2] Johnson L F 1962 *J. Appl. Phys.* **33** 756
[3] Bagdasarov Kh, Voronko Yu K, Kaminskii A A, Krotova L V and Osiko V V 1965 *Phys. Stat. Sol.* **12** 905
[4] Kaminskii A A, Osiko V V and Voronko Yu K 1967 *Phys. Stat. Sol.* **21** 17
[5] Kaminskii A A, Sobolev B P, Bagdasarov Kh S, Fedorov P P, Kevorkov A M, Seyranyan K B and Sarkisov S E 1974 *Phys. Stat. Sol.* **26** K63
[6] Bagdasarov Kh, Voronko Yu K, Krotova L V, Kaminskii A A and Osiko V V 1965 *Phys. Stat. Sol.* **12** 905
[7] Voronko Yu K, Kaminskii A A and Osiko V V 1966 *Izv. Akad. Nauk SSSR, Neorg. Mater.* **2** 1161
[8] Wang Q G, Su L B, Li H J, Zheng L H, Guo X, Jiang D P, Zhao H Y, Xu J, Ryba-Romanowski W, Solarz P and Lisiecki R 2011 *J. Alloy. Compd.* **509** 8880
[9] Siebold M, Bock S, Schramm U, Xu B, Doualan J L, Camy P and Moncorgè R 2009 *Appl. Phys. B* **97** 327
[10] Pollack S A 1964 *J. Chem. Phys.* **40** 2751
[11] Voronko Yu K and Sychugov V A 1968 *Phys. Stat. Sol.* **25** K119
[12] Labe C, Doulan J L, Camy P, Moncorgè R and Thuau M 2002 *Opt. Commun.* **209** 193
[13] Meng Z, Yoshimura T, Fukue K, Higashihata M, Nakata Y and Okada T 2000 *J. Appl. Phys.* **88** 2187
[14] Tan M C, Kumar G A and Riman R E 2009 *Opt. Express* **17** 15904
[15] Xu J, Su L B, Li H J, Zhang D, Wen L, Lin H and Zhao G J 2007 *Opt. Mater.* **29** 932
[16] Wang Q G, Su L B, Zheng L H, Li H J, Tang H L, Guo X, Jiang D P and Xu J 2012 *J. Am. Ceram. Soc.* **95** 972
[17] Kumar G A, Riman R, Chae S C, Jang Y N, Bae I K and Moon H S 2004 *J. Appl. Phys.* **95** 3243
[18] Xu J W, Zhou Y Z, Zhou G Q, Xu K, Deng P Z and Xu J 1998 *J. Cryst. Growth* **193** 123
[19] Ravel B 2005 *Phys. Scr.* **115** 1007
[20] Judd B R 1962 *Phys. Rev.* **127** 750
[21] Ofelt G S 1962 *J. Chem. Phys.* **37** 511
[22] Carnal W T, Crosswhite H and Crosswhite H M 1978 *Energy Level Structure and Transition Probabilities in the Spectra of the Trivalent Lanthanides in LaF_3*
[23] *The Merck Index*, 10th ed., 1983, edited by M Windholz, S Budavari, R F Blumetti, and E S Otterbein (Merck & Co., INC)
[24] Cockroft N J, Thompson D, Jones G D and Syme R W G 1987 *J. Chem. Phys.* **86** 521
[25] Petit V, Camy P, Doualan J L, Portier X and Moncorgé R 2008 *Phys. Rev. B* **78** 085131
[26] Greis O and Bevan D 1978 *J. Solid State Chem.* **24** 113
[27] Bendall P, Catlow C and Fender B 1981 *J. Phys. C* **14** 4377
[28] Petit V, Doualan J, Camy P, Ménard V and Moncorgé R 2004 *Appl. Phys. B* **78** 681
[29] Catlow C R A, Chadwick A V, Greaves G N and Moroney L M 1984 *Nature* **312** 601
[30] Nicolov M 2000 *J. Cryst. Growth* **218** 62